Estimation of turbulence intensity using rotor effective wind speed in Lillgrund and Horns Rev-I offshore wind farms

Gögmen, Tuhfe; Giebel, Gregor

Published in:
Renewable Energy

Link to article, DOI:
10.1016/j.renene.2016.07.038

Publication date:
2016

Document Version
Publisher's PDF, also known as Version of record

Renewable Energy 99 (2016) 524–532

Contents lists available at ScienceDirect

Renewable Energy

journal homepage: www.elsevier.com/locate/renene

Estimation of turbulence intensity using rotor effective wind speed in Lillgrund and Horns Rev-I offshore wind farms

Tuhfe Göçmen*, Gregor Giebel

Technical University of Denmark, Department of Wind Energy, Risø Campus, Roskilde, Denmark

ARTICLE INFO

Article history:
Received 2 September 2015
Received in revised form
27 June 2016
Accepted 16 July 2016

Keywords:
Turbulence intensity
Rotor effective wind speed
Real-time wind farm calculations

ABSTRACT

Turbulence characteristics of the wind farm inflow have a significant impact on the energy production and the lifetime of a wind farm. The common approach is to use the meteorological mast measurements to estimate the turbulence intensity (TI) but they are not always available and the turbulence varies over the extent of the wind farm. This paper describes a method to estimate the TI at individual turbine locations by using the rotor effective wind speed calculated via high frequency turbine data.

The method is applied to Lillgrund and Horns Rev-I offshore wind farms and the results are compared with TI derived from the meteorological mast, nacelle mounted anemometer on the turbines and estimation based on the standard deviation of power. The results show that the proposed TI estimation method is in the best agreement with the meteorological mast. Therefore, the rotor effective wind speed is shown to be applicable for the TI assessment in real-time wind farm calculations under different operational conditions. Furthermore, the TI in the wake is seen to follow the same trend with the estimated wake deficit which enables to quantify the turbulence in terms of the wake loss locally inside the wind farm.

1. Introduction

The turbulence characteristics in a wind farm are important in estimating the power production and the loads on the wind turbines. As the wind farms increase in size, particularly offshore, a good description of the wakes becomes crucial for an accurate performance prediction of the wind farm. The atmospheric turbulence enhances the wake recovery while together with the wake-induced turbulence, they are the major source of fatigue loading on the wind turbines [1]. Both the atmospheric and the wake added turbulence are parametrised in various wake models in terms of Turbulence Intensity (TI) [2–6] which is defined by

$$TI = \frac{\sigma_U}{U}, \tag{1}$$

where U is the wind speed and σ_U is the standard deviation of the wind speed.

In wind farm calculations, the best possible way to estimate the TI is to use the standard deviation and the mean of the wind speed over 10 min intervals measured by a meteorological mast (met mast). However, those measurements do not provide the accurate TI at the turbine position since they are located elsewhere and, depending on the wind direction, the measurements might be in the wake of the wind farm or any other obstacle. Also in some cases, often after the turbines started operating, the met mast measurements are not available or they can not be used due to data issues [7,8]. On the other hand, to estimate the turbulence in the wake either advanced, computationally expensive numerical simulations or parametrised correlations fitted to the experimental data are in use, depending on the distance from the upstream turbine [9]. Here we propose another method to estimate the TI using the turbine data which is applied to the Lillgrund and Horns Rev I offshore wind farms. The results are compared with the TI derived from the met mast measurements as well as the standard deviation of the nacelle anemometer wind speed and the power fluctuations. Both the atmospheric and wake added TI are calculated using the rotor effective wind speed algorithm which was developed to estimate the wind speed using operational supervisory control and data acquisition (SCADA) system. It was designed to be used in real-time wind farm calculations that are required to perform control strategies and follow the balancing market regulations. The effective wind speed algorithm was validated on Horns Rev and Thanet wind

* Corresponding author.
E-mail address: tuhf@dtu.dk (T. Göçmen).

http://dx.doi.org/10.1016/j.renene.2016.07.038
0960-1481/

farms for both normal operation and down-regulation conditions [6].

For the Lillgrund test case, an additional Siemens turbine SCADA signal called "WindEstimate" is considered as the wind speed to estimate the TI at the turbine locations. The "WindEstimate" was introduced to have a signal with smaller fluctuations, and one that is less sensitive to turbine curtailments than the anemometer signal. The signal is calculated by generating a look-up table for the produced power in terms of the rotor averaged wind speed, rotational speed and pitch angle together with the original rotor geometry. The look-up table is then used considering the operational power, rotational speed and pitch to interpolate the wind speed when the turbine is online.

2. Sites and data

2.1. Lillgrund offshore wind farm

The Lillgrund wind farm is located in Øresund area, between Sweden and Denmark, 6–8 km from the Swedish west coast; south of Malmø. It consists of 48 S SWT-2.3-93 wind turbines with a total rated capacity of 110 MW. The turbine diameters are 93 m and the hub is located at 65 m height. The layout of the Lillgrund is rather unusual due to a gap in the middle of the farm, and the quite small internal spacings of the turbines of 3.3 and 4.3 rotor diameters, D, as shown in Fig. 1(a). The power and thrust curves of the Simens turbines on the site are shown in Fig. 1(b)).

The data used in the calculations cover a period of 7 months, from 06/2012 to 01/2013, with a sampling rate of 1 Hz. On the met mast, the closest sensors to the hub height of the turbines are taken into account therefore the second-wise wind speed measurements are taken at 65 m while the wind direction and temperature are observed at 61 m. The wind rose in Fig. 2(a) of the met mast data shows the pattern of the prevailing winds, mainly westerly during the considered period. The second-wise extracted signals from the SCADA system are active power, pitch angle, rotational speed, and nacelle anemometer wind speed, where the first three are used to calculate the rotor effective wind speed. Additionally, the Siemens "WindEstimate" signal (SiemensWS) is received from the turbines in question and it is first used in the estimated wind speed comparison and then in the TI calculations.

2.2. Horns Rev I offshore wind farm

The Horns Rev wind farm is located 14 km away from the west coast of Denmark and consists of 80 Vestas V80 turbines with a total capacity of 160 MW. The layout of the wind farm together with the locations of the 2 of the surrounding met masts ($M2$, $M6$) is shown in Fig. 3(a).

Note that, the fundamental model validation for the TI estimation using the SCADA data is performed using relatively longer period of met-mast and turbine data in Lillgrund. However, since the Lillgrund SCADA data is limited to a few number of turbines in a row, the model is also implemented in Horns Rev-I wind farm with 80 turbines available for illustration purposes and to discuss the applicability of the model to larger scales.

For the Horns Rev case, the SCADA signals used to calculate the TI at the turbine locations are not continuous and include the period of 04/10–10/10, 14/10–21/10, 03/11–10/11 and 18/11–19/11 in 2013, 21 days in total. The implementation of the TI estimation algorithms on such short-term data might provide insight on the operational wind characteristics in the area as emphasized in the studies of Longley et al. [10] and Chan [11]. In order to assess if the 21 days of data in question is adequate to evaluate the model performance in estimating the turbulence levels, the uncertainty of the variances among the time series are quantified using approximations proposed by Lenschow et al. [12,13]. The relative systematic and random errors of the second order moment of the rotor effective wind speed, which is described in Section 3, are calculated at the turbine positions for the 21 days period, as shown in Equations (2) and (3), respectively.

$$\frac{F-\langle F(T)\rangle}{F}\approx 2\frac{\tau}{T} \tag{2}$$

$$\frac{\sigma_F(T)}{|F|}\approx 2\sqrt{\frac{\tau}{T}} \tag{3}$$

where F is the second order moment, or the flux, of the rotor effective wind speed, T is the length of the time series in question, σ_F is the standard deviation of the random error of the flux and τ is the integral time scale defined as in Equation (4).

$$\tau=\int_0^T \rho(t)dt \tag{4}$$

$\rho(t)$ being the autocorrelation function. Note that the approximations are derived in Ref. [12] where $T\gg\tau$, which is clearly satisfied where $0.506\leq\tau\leq 15.651$ among the turbine locations.

Along the wind farm, the systematic error differs from 0.0335% to 1.035% for the investigated time interval, thus considered

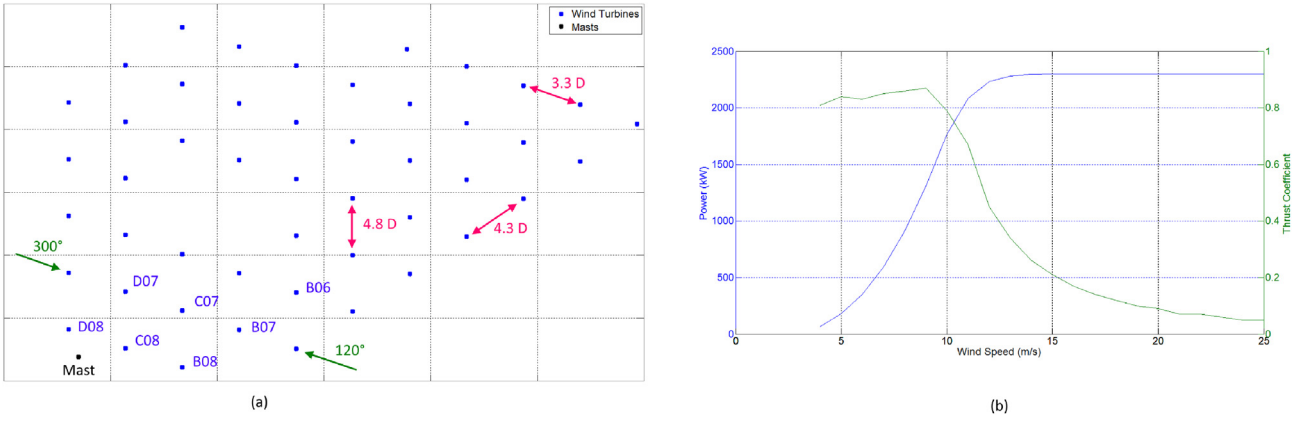

Fig. 1. (a) Layout of the Lillgrund offshore wind farm and (b) Siemens SWT-2.3-93 turbine power, P, and thrust, c_T, curve.

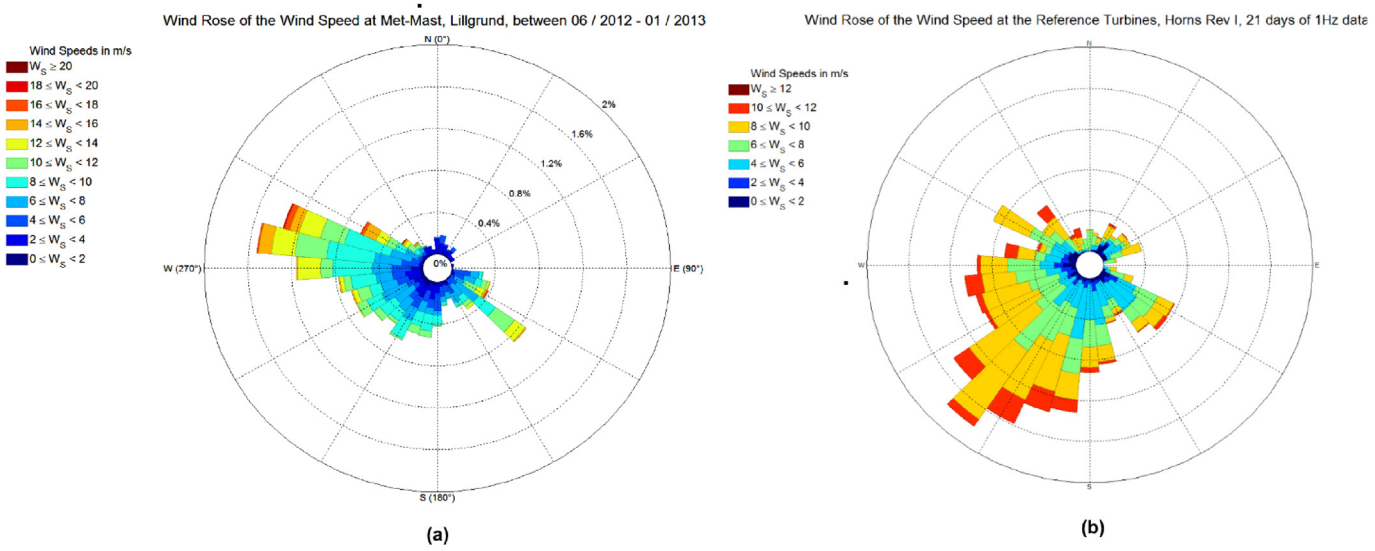

Fig. 2. Wind rose of the offshore sites, wind speed observed at (a) Lillgrund – the met mast location at 61 m from 06/2012 to 01/2013, 7 months in total (b) Horns Rev I – the upstream reference turbine(s), covering a period of 21 days in total.

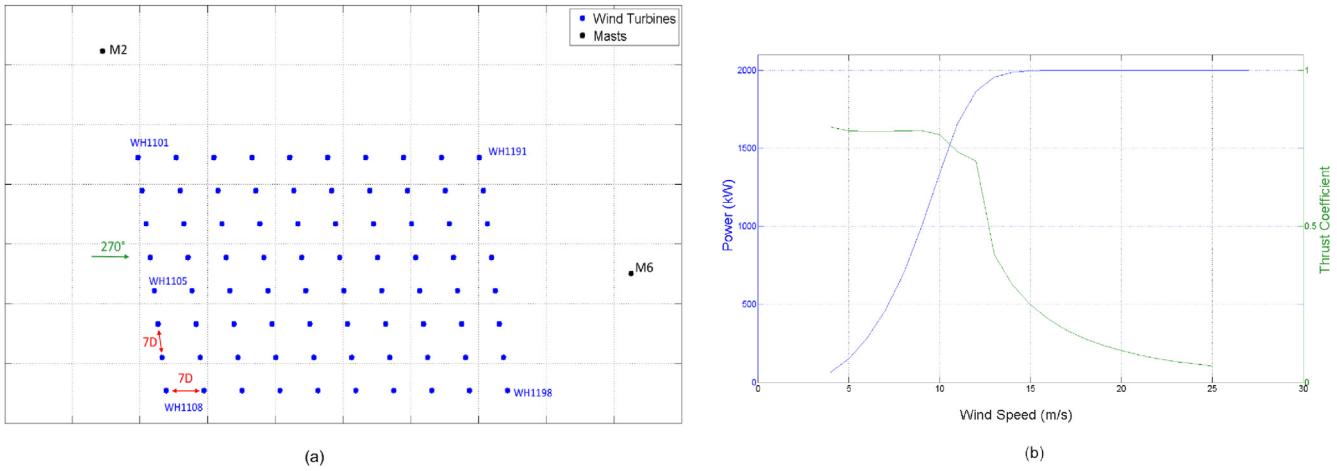

Fig. 3. (a) Layout of the Horns Rev I offshore wind farm and (b) Vestas V80-2MW offshore turbine power, P, and thrust, c_T, curve.

negligible. On the other hand, the relative random error of the second order moment of the rotor effective wind speed is estimated to be between 1.829%–10.174% throughout the wind farm, which is significantly larger than the systematic error but still ≤10% level. Therefore, the considered 21 days period is found adequate to estimate the turbulence levels at the turbine locations inside Horns Rev-I.

Similar to the Lillgrund case, the active power, pitch angle, rotational speed, and nacelle anemometer wind speed signals are extracted from all the turbines together with the yaw signals. It can be seen from Fig. 2(b) that the main wind direction recorded at turbine WH1105 during the considered period is south-west. Since there are no available met mast data recorded at the same period, the atmospheric TI is not compared to the met mast but instead, the change in the TI through the wind farm is investigated.

3. High frequency rotor effective wind speed

The common approaches to estimate the wind speed at the turbine location(s) are either to use the power production together with the power curve (power curve wind speed) [14] or the nacelle anemometer (nacelle wind speed) [15]. The power curve wind speed is not applicable outside the region between cut-in and rated wind speed as well as for different operational conditions, e.g. down-regulation, where the optimal power curve is no longer valid. The nacelle wind speed can induce unacceptable uncertainties especially for real-time calculations during shorter periods [16]. In order to estimate the wind speed at the turbine locations, the proposed methodology considers power, P, pitch angle, θ, and rotational speed, ω, together with the general power expression, which is

$$P = \frac{1}{2}\rho C_P(\lambda,\theta)\pi R^2 U^3, \tag{5}$$

where ρ is the air density, λ is the tip speed ratio, R is the rotor radius, and U is the incoming wind speed.

Since C_P does not follow the optimal curve during off-performance conditions and the look-up tables are a matter of confidentiality, the generic pitch angle and tip speed ratio dependence of power coefficient proposed by Heier [17] is applied to

simulate the $C_P(\theta, \lambda)$, see equation set 6. In Göçmen et al. [6], the rotor effective wind speed estimation approach is described in detail and applied to data from Horns Rev-I wind farm and NREL 5 MW turbine simulations, under different operational conditions. In Fig. 4, the rotor effective wind speed is implemented in Lillgrund and compared with the power curve, nacelle wind speed and Siemens estimated wind speed as well as the high frequency (1 Hz) met mast wind speed observations.

$$C_P(\lambda,\theta) = c_1\left(\frac{c_2}{\lambda_i} - c_3\theta - c_4\theta^{c_5} - c_6\right)exp\left(\frac{-c_7}{\lambda_i}\right)$$
$$\lambda_i = \left[\left(\frac{1}{\lambda + c_8\theta}\right) - \left(\frac{c_9}{\theta^3+1}\right)\right]^{-1} \quad (6)$$

Fig. 4 shows that the fluctuations in point measurements (i.e. the nacelle and met mast wind speed) are a lot larger than the others. Due to the geometrical (or volume) averaging embedded in the power curve wind speed, Siemens estimated wind speed and rotor effective wind speed, the scatter is smaller. Moreover, since those rotor averaged wind speeds use active power as an input, they seem inefficient to simulate lower range wind speeds around the cut-in. It is also seen that the power curve wind speed is not applicable for the wind speeds in the rated region, i.e. above 13 m/s. The geometrical average also explains the better agreement seen between the three local wind speed estimation methods. The developed rotor effective algorithm is seen to successively reproduce the wind speed estimated using the authentic $C_P(\lambda, \theta)$ table of the Siemens SWT − 2.3–93 turbine with a slight underestimation around the rated wind speed where the pitch peaks. The only significant deviation between those two outputs occurs where the pitch is around $\theta = -1°$, due to the sensitivity in the developed algorithm, see equation set 6. It should be noted that the Siemens wind speed data is filtered for the turbine operational state.

4. Atmospheric turbulence intensity

The atmospheric turbulence levels are generally lower offshore than over land and the typical TI values offshore are 6–8% [8]. Low atmospheric turbulence, together with stable conditions, tends to delay the wake recovery and does not necessarily mean less structural loading on the turbines since the wake added turbulence plays an important role. Therefore, also in the offshore wind farm calculations the TI is considered to be an important parameter [18].

The TI calculated using the 1 Hz met mast measurements for a period of 7 months is compared to the upstream turbine data in Lillgrund. Using 1 Hz SCADA data, the atmospheric TI is computed using; 1) the nacelle anemometer measurements, 2) Siemens estimated wind speed, 3) rotor effective wind speed, and 4) the standard deviation of the active power signal from the most upstream turbine(s) in equation (1). The implementation of the first three methods is fairly straight-forward. In the last approach, the standard deviation of the active power is correlated to the standard deviation of the wind speed using the method developed by Jørgensen et al. [19] based on Thomsen and Petersen [20], as

$$\sigma_P = B\sigma_U\left(\frac{dP}{dU}\right)_{U_{pow}}, \quad (7)$$

where σ_P is the 10-min standard deviation of the active power signal sampled at 1 Hz, B is a constant typically ranges between $0.8 - 0.9$, depending on the mean wind speed, P is the active power and U is the wind speed. The slope $\left(\frac{dP}{dU}\right)_U$ is calculated using the

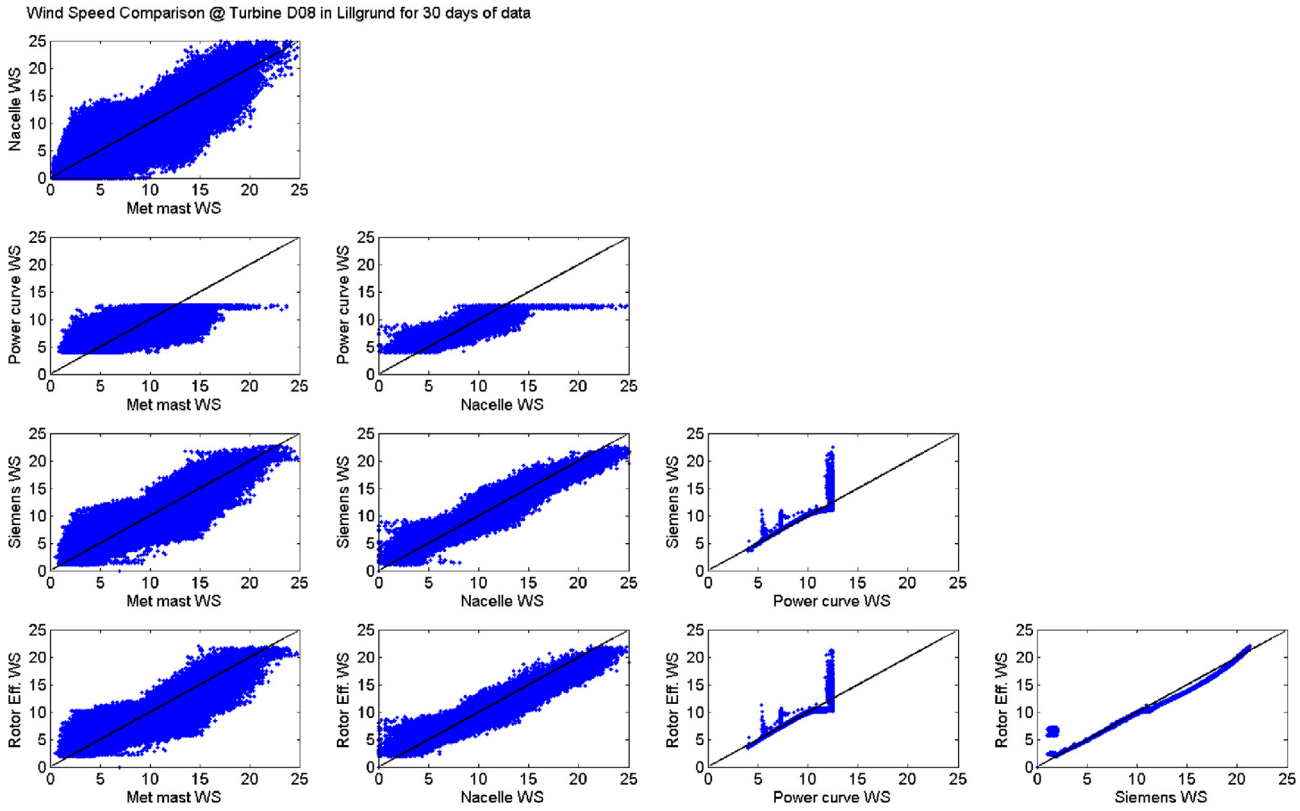

Fig. 4. Second-wise Wind speed comparison of the measurements taken at the met mast (Met mast WS) and the nacelle anemometer (Nacelle WS) with the estimations using the turbine power curve (Power curve WS), using the manufacturer $C_P(\lambda, \theta)$ (Siemens WS) and using the approximated $C_P(\lambda, \theta)$ [6] (Rotor eff. WS).

manufacturer's power curve and the mean power curve wind speed. Therefore, it is important to note that the difference between the operational power curve and the manufacturer's power curve affects the results. Additionally, the method is only applicable where the slope, $\left(\frac{dP}{dU}\right)_{U_{pow}}$ is other than zero and the turbine is operational, i.e. between the cut-in and rated wind speeds, 4–13 m/s for SWT − 2.3–93 offshore wind turbine.

In order to approximate the constant B, the methodology proposed by Barthelmie et al. [21] is implemented as

$$B = \frac{\sigma_P}{\left(\frac{dP}{dU}\right)_{U_{pow}} U_{pow} TI_{metmast}}, \quad (8)$$

where the TI calculated by the power fluctuations (TI_{pow}) is assumed to be equal to the TI calculated using the met mast measurements ($TI_{metmast}$). Averaging results between 5 and 12 m/s, using another dataset from Lillgrund covering 3 years period (from 01/2012 to 01/2015), gives $B = 0.744$ which is considered in both the atmospheric and the wake induced turbulence calculations.

In Fig. 5, the ambient TI is calculated using the met mast together with the power measurements, nacelle anemometer (TI_{nws}), Siemens estimated wind speed ($TI_{SiemensWS}$), and rotor effective wind speed (TI_{effWS}) at turbine $D08$. The results are averaged over 1 m/s bins between 4.5 and 15.5 m/s for all the wind directions in the top figure and; over 5° wind direction bins for all the wind speeds in the bottom figure where $TI_{metmast}$ is presented with 95% confidence level normalized with respect to the number of data points in the interval.

It can be seen from both Fig. 5(a) and (b) that the TI is overestimated by the nacelle anemometer wind speed. Although the TI_{pow} is in a good agreement with the met mast for low speed flows, around the rated wind speed it rapidly increases due to the behaviour of the power curve. The TI_{effWS} on the other hand, seems to be successfully representing the characteristics of the $TI_{metmast}$ with a consistent under-estimation similar to the Siemens estimated wind speed. That difference can be explained by the fact that the $TI_{metmast}$ is calculated using the point measurements whereas the TI_{effWS} and $TI_{SiemensWS}$ are considering the wind speed seen by the whole rotor. That automatically includes the geometrical averaging between 21.5 m–114.5 m, which smooths out the fluctuations in wind speed. Where the wind direction is between 100 − 120° and 320 − 340° in Fig. 5(b), the results of the TI_{effWS} and $TI_{metmast}$ are diverse due to the location of the turbine $D08$ and the met mast, where the met mast is affected by the wake – see Fig. 1. Note that the TI measured by the met mast in the wake is much higher than the atmospheric TI which will be discussed later in detail.

5. Turbulence intensity in wind turbine wakes

Downstream of a turbine, in addition to the atmospheric turbulence the wake induced turbulence should also be taken into account. While increasing TI corresponds to higher mixing and therefore reduced wake losses, its impact on the fatigue loading of the downstream turbine(s) is significant mainly due to the partial wakes [22].

Since the atmospheric TI calculations show that the rotor estimated wind speed gives the best TI estimate, the other TI calculation methods are not implemented in the added wake calculations. The turbulence at the downstream turbine positions are estimated using only the rotor effective wind speed for both of the wind farms.

5.1. Wake added TI in Lillgrund

The 1-sec turbine data in Lillgrund is extracted from the turbines indicated in Fig. 1(a). For the calculations of the TI in the wake,

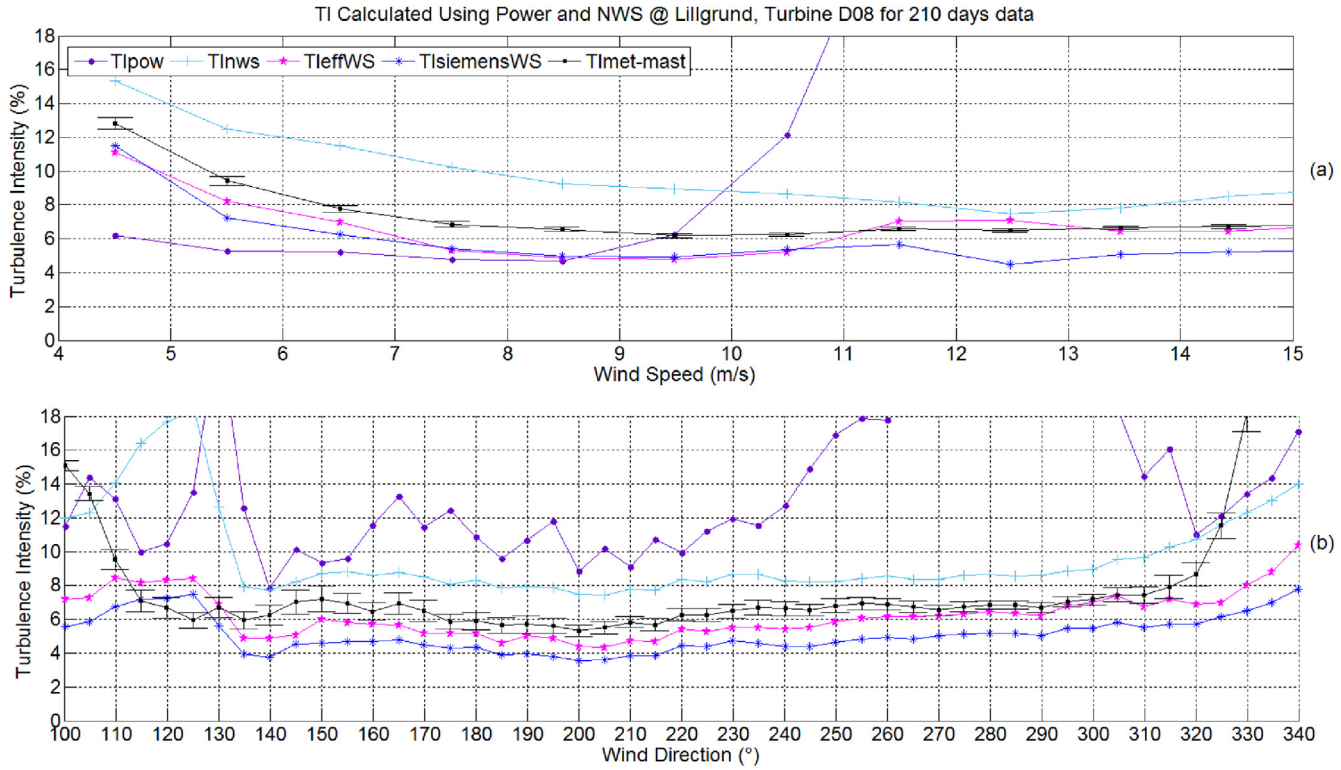

Fig. 5. Ambient Turbulence Intensity in Lillgrund, presented in terms of (a) the wind speed (b) the wind direction, errorbars indicating 95% normalized confidence intervals.

Row 8 (D08, C08, B08) with 3.3*D* and Row B (B08, B07, B06) with 4.3*D* turbine spacings are analysed and compared with the met mast data.

Fig. 6(a) clearly shows the effects of the wake along the wind directions 120 ± 10° and 300 ± 15° where the turbine B08 is the most upstream turbine around 120° and the most downstream around 300°. Outside of that interval, the TI is almost identical between the turbines and corresponds to the atmospheric turbulence, as in Fig. 5. During both of the south-east and north westerly winds, the TI seems to be the highest at the second turbine in the row even though the third turbine is exposed to a double wake. This behaviour is in line with the wake deficit calculations performed as a benchmark case in Ref. [23] where the wake deficit at the second turbine is visibly higher than the third and it remains approximately constant among the rest of the turbines in the row. To understand the relation between the TI and the local wake losses, the standard deviation and the mean wind speed are investigated separately. It can easily be seen in Figs. 7(a) and 6(a) that the standard deviation and the TI have the same pattern where the wake loss directly affects the difference between the upstream and downstream turbulence levels. In the first wake in Fig. 7(b), i.e. around 120°, the deficit is much higher than the second wake around 300° due to the difference between the thrust coefficient for upstream wind speed of 9 m/s and 10 m/s, see Fig. 1(b).

The effects of the wake to the turbulence is observed to be significant such that the difference between the wake and atmospheric TI is up to 7% for the 3.3*D* spacing case. Also note that the met mast is in the wake of the neighbouring turbines before 115° and after 315° wind directions.

The southernmost three turbines along Row B encounter 5 events where the effects of the wake on the TI are observed for the incoming wind directions between 100 – 340°, see Fig. 6(b). For the first event between 120 ± 15°, both turbines B07 and B06 are exposed to a single wake thus have almost identical values. For the second one between 180 ± 15° though, both turbine B08 and B07 are upstream and B06 is under the effect of a single wake. The third event is along the perpendicular direction to the row, 222 ± 15° causing the highest increase in the TI at the location of the second turbine. Interestingly, between 260 ± 15° turbines B07 and B06 are subjected to the same turbulence where the former has 4 upstream turbines and the latter has 3 which is also similar to the wake deficit trend in Ref. [23]. Similarly between 300 ± 10°, the estimated TI is almost identical at turbines B06, B07 and B08 where they have 5, 4 and 3 turbines upstream, respectively. The behaviour of the TI in multiple wakes is presented in Fig. 8 for the perpendicular direction when turbine – turbine spacing is 3.3*D*. Fig. 8 shows that the turbulence level increases significantly at the first upstream turbine and it is much higher for a single wake compared to a double wake. Although the number of wake data are limited, it is also seen that the existence of three or four upstream turbines hardly makes any difference which will be discussed utilizing more turbines further upstream with larger spacing for the Horns Rev case, Fig. 9.

5.2. Wake added TI in Horns Rev I

In Horns Rev, the data from all the turbines are available for the considered period of 21 days therefore a 'turbulence contour' through the wind farm can be constructed. Note that, Fig. 10 is built based on the linearity assumption between the turbine locations where the information is in fact limited to individual turbine swept areas. The observation of the actual behaviour in between the turbines are left as a future work where detailed measurements

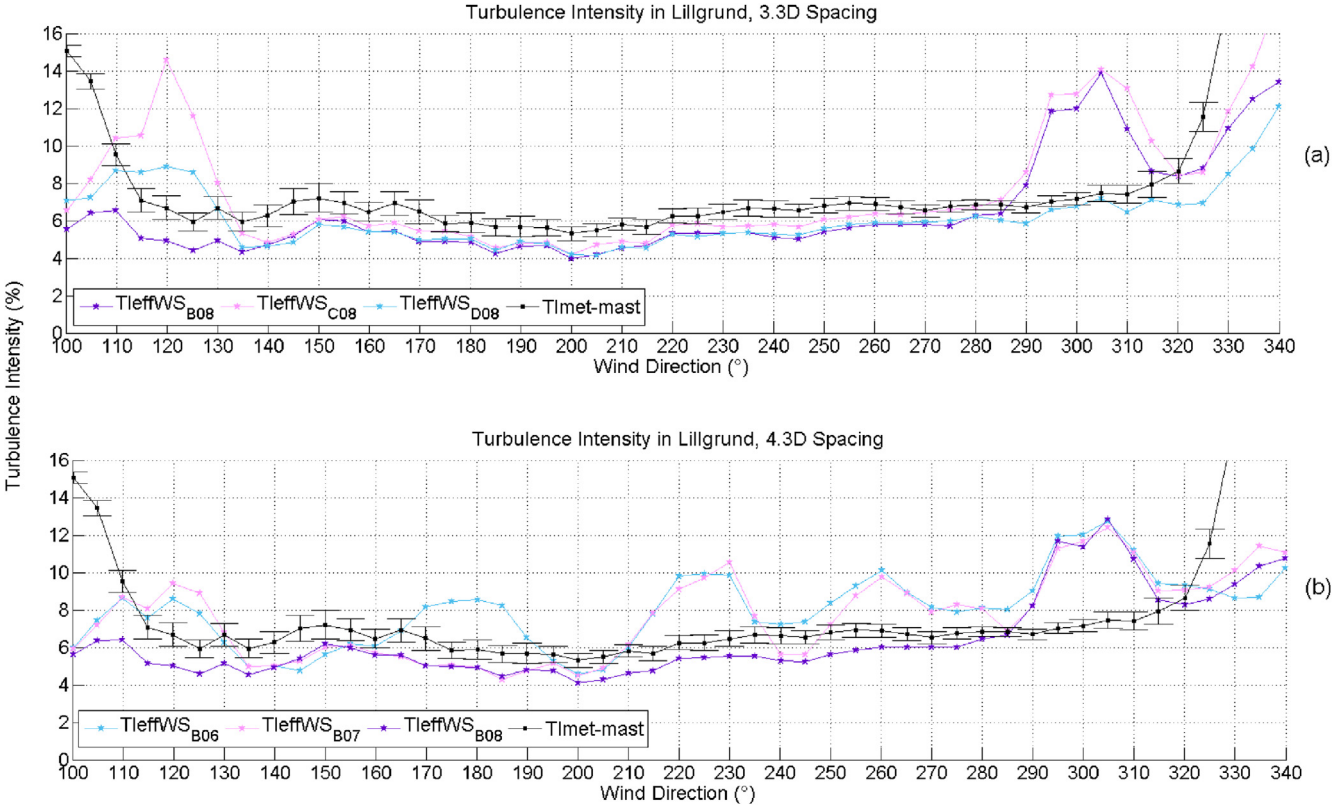

Fig. 6. Turbulence Intensity in the wake, estimated using the rotor effective wind speed along (a) Row 8 – 3.3*D* spacing (b) Row B – 4.3*D* spacing, averaged over 5° wind direction bins, errorbars indicating 95% normalised confidence intervals.

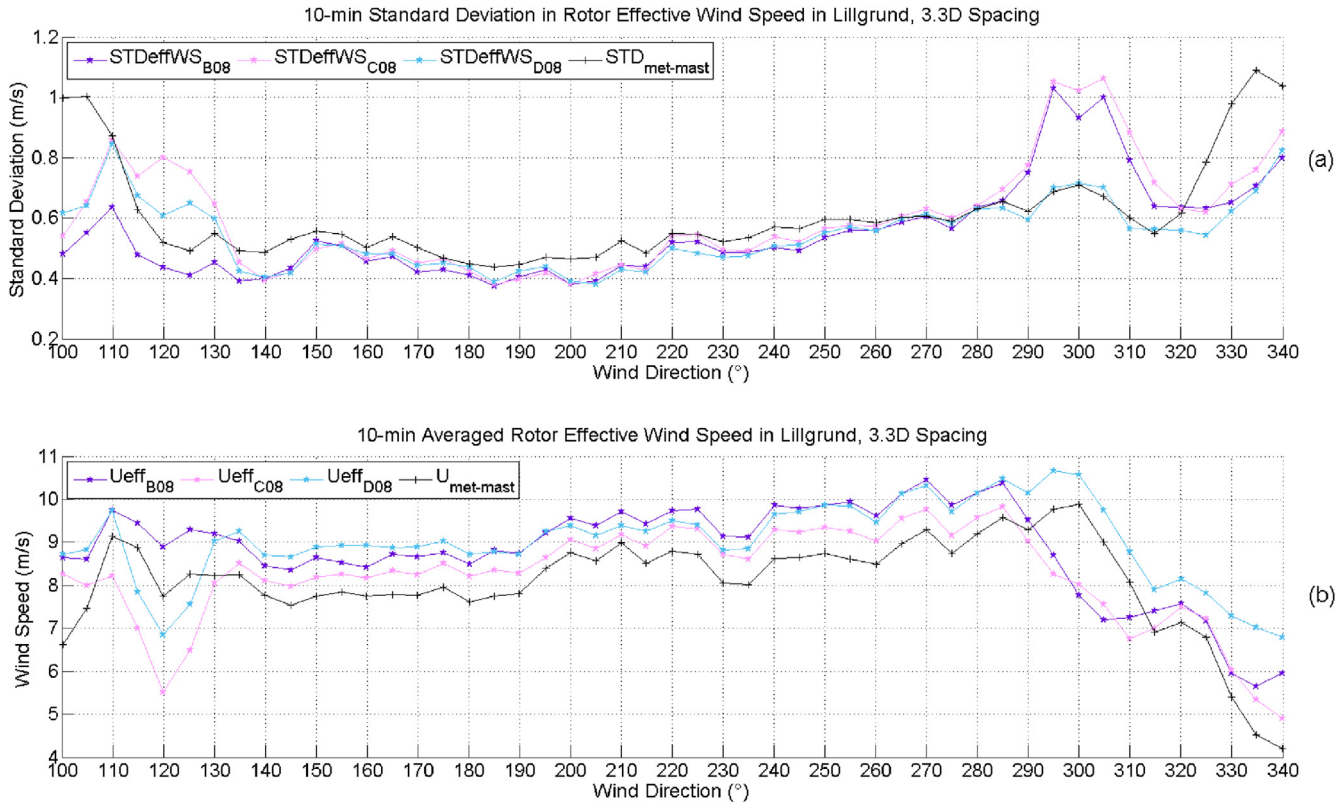

Fig. 7. The components of the TI in Lillgrund along Row 8 – 3.3*D* spacing (a) 10-min standard deviation in rotor effective wind speed (b) 10-min mean wind speed, averaged over 5° wind direction bins, errorbars indicating 95% normalised confidence intervals.

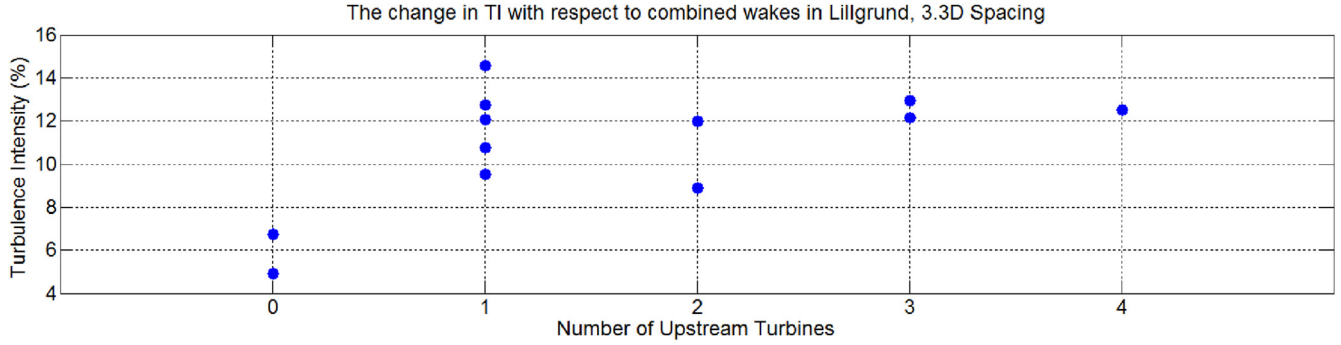

Fig. 8. The behaviour of TI in Lillgrund with respect to combined wake effects, 3.3*D* spacing along perpendicular 120° and 300° wind directions.

have to be carried out.

The TI presented in Fig. 10(a) is calculated using the 10-min standard deviation and the mean of the 1-sec rotor effective wind speed and averaged over the upstream wind direction bin 210° ± 15°. The wake loss in Fig. 10(b) is calculated using the same dataset with the linearized computational fluid dynamics model Fuga [24] for the same wind direction sector and neutral atmospheric stability. The wind speed and direction from the turbine WH1105 is taken as references where the wake loss is calculated in percentages as $U_{wake}/U = (1 - U_{wake}/U_{ref}) \cdot 100$.

Fig. 10(b) and (c) show that the behaviour of the TI follows a very similar trend as the wake deficit such that the turbines with higher loss, thus lower local wind speed, are exposed to higher turbulence. However, their behaviours are not identical due to the simplifications in the employed wake model in which the local wind direction and speed is not taken into account and the calculations are based on the reference wind speed and direction. Still, some of the non-homogeneity is captured inside the wind farm since the directional averaging is applied considering the meandering. Similar to the Lillgrund case, the 10-min standard deviation in wind speed and the added turbulence are not consistently increasing with the superposed wake. Fig. 9 shows that the turbulence increases the most at the first downstream turbine also, then remains within a certain zone with a slight tendency to increase after the fourth turbine for westerly winds. The pattern of the TI along a single row of turbines is highly analogous to the power deficit measurements in Horns Rev for westerly winds as illustrated by Hansen et al. [7]. Both the TI and the wake loss analyses show that the flow direction at the turbine location plays an important role in defining the trend of the turbulence increases throughout the wind

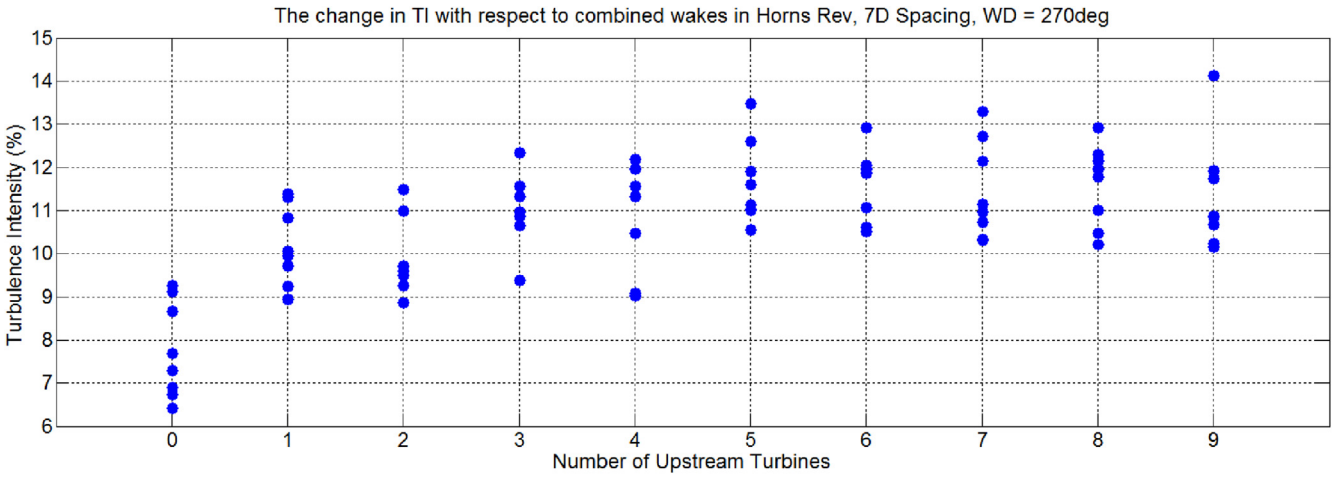

Fig. 9. The behaviour of TI in Horns Rev with respect to combined wake effects, 7*D* spacing along perpendicular westerly winds, 270°.

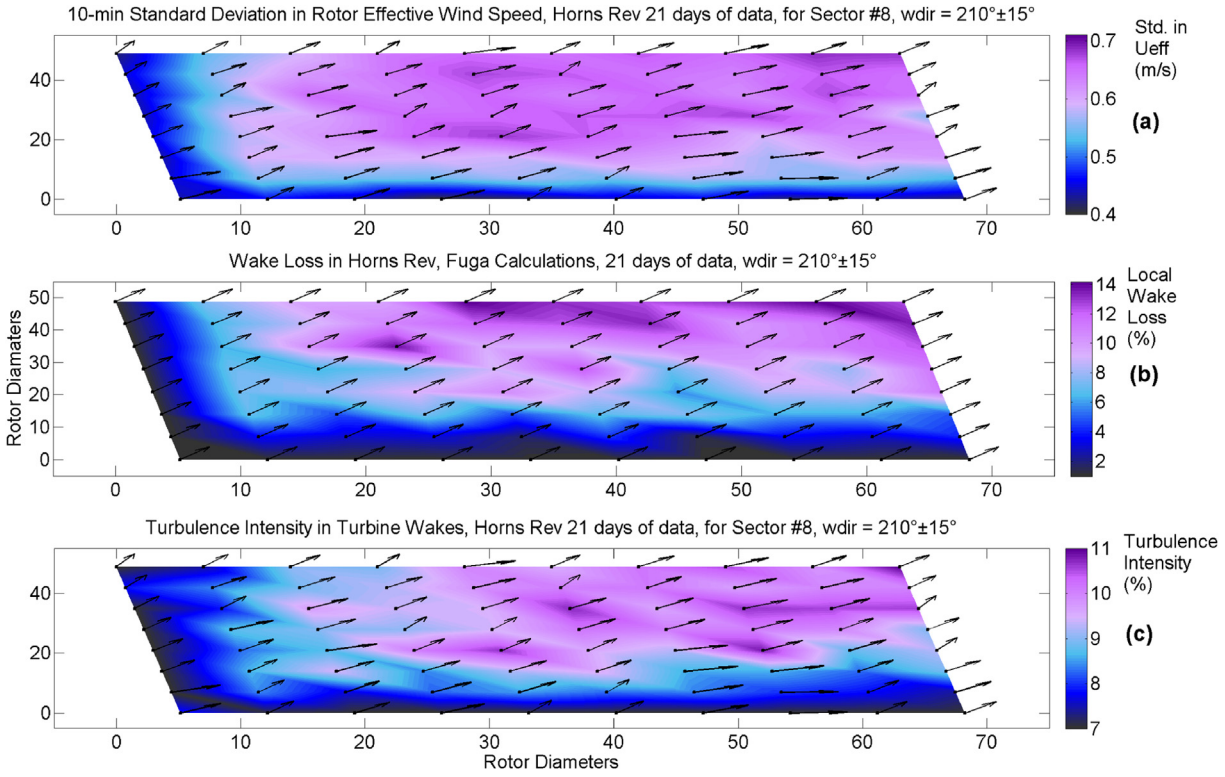

Fig. 10. (a) 10-min standard deviation in wind speed, (b) The wake loss, calculated using Fuga [24], (c) The turbulence intensity along the Horns Rev I offshore wind farm, arrows indicate the mean wind direction(s) read by the models filtered across 210° ± 15° bin (see 2(b)).

farm, as it sets the direction of the local wake.

6. Conclusions

To comprehend the atmospheric and wake induced turbulence is crucial for wind farm calculations to estimate the power production and the structural loading on wind turbines. Therefore, here we present a methodology to estimate the TI across the wind farm based on the rotor effective wind speed calculated using the turbine data. The methodology is implemented in Lillgrund and Horns Rev-I offshore wind farms and compared with the met mast as well as the nacelle anemometer and standard deviation of the produced power.

In Lillgrund, the proposed method estimates the atmospheric TI consistently lower than the met mast, by 1.6% for the analysed data with an averaged wind speed 7.7 m/s. Such discrepancy is to be expected since the met mast provides point measurements and the proposed method characteristically includes geometrical averaging over the rotor. Nevertheless, it is shown to produce closer results to the met mast TI compared to the TI derived from the Siemens "WindEstimate" SCADA signal and unlike the one derived using the standard deviation of power, it is applicable also at rated region or under curtailment. The nacelle wind speed measurements on the other hand, over-estimate the atmospheric TI by up to 3.7%

compared to the met mast, depending on the wind speed. The performance of the method to approximate the TI in the wake is evaluated using two different rows of 3 turbines with 3.3D and 4.3D spacings where a higher increase in TI is perceived along the first downstream turbine(s). The results show that in both cases, during perpendicular flows the second turbine is exposed to the highest TI whereas the turbulence levels in the wake of 4 and 5 turbines are very similar. The increase in the TI along the rows is found to be highly correlated to the wake deficit trend observed in the same wind farm.

The short-term TI behaviour across Horns Rev is investigated using the rotor effective wind speeds and compared to the wake loss calculated using linearized CFD model Fuga. The south-westerly wind direction bin averaged results clearly show that the local TI is directly proportional to the wake loss, as observed in the Lillgrund case. The parametrisation of the added wake TI in terms of the local wake loss in offshore wind farms is left as a future work.

Acknowledgements

The author would like to thank Michael Støttrup from Siemens Wind Power, Brande, Denmark for provision of the 1 Hz data in Lillgrund offshore wind farm, clarifications of Siemens SCADA system and the revision of this work which is a part of the PossPOW Project: Possible Power of Offshore Wind power plants, funded by Energinet.dk under the Public Service Obligation (contract number 2012-1-10763).

References

[1] S.T. Frandsen, Turbulence and Turbulence-generated Structural Loading in Wind Turbine Clusters, Risø-R-1188(EN), Risø National Laboratory, 2007.
[2] M.P. van der Laan, N.N. Sørensen, P.-E. Réthoré, J. Mann, M.C. Kelly, N. Troldborg, J.G. Schepers, E. Machefaux, An improved $k-\varepsilon$ model applied to a wind turbine wake in atmospheric turbulence, Wind Energy 18 (5) (2015) 889–907.
[3] G.C. Larsen, A Simple Stationary Semi-analytical Wake Model, risø-r-171, 2009. Tech. rep., Risø, Denmark.
[4] G.C. Larsen, H. Madsen Aagaard, F. Bingöl, J. Mann, S. Ott, J.N. Sørensen, V. Okulov, N. Troldborg, N.M. Nielsen, K. Thomsen, Dynamic Wake Meandering Modeling, Risø-R-1607(EN), Risø National Laboratory, 2007.
[5] J.F. Ainslie, Calculating the flowfield in the wake of wind turbines, J. Wind Eng. Ind. Aerodynam. 27 (1) (1988) 213–224.
[6] T. Göçmen Bozkurt, G. Giebel, N.K. Poulsen, M. Mirzaei, Wind speed estimation and parametrization of wake models for downregulated offshore wind farms within the scope of PossPOW project, J. Phys. Conf. Ser. 524 (2014) 12156–12162. IOP Publishing.
[7] K.S. Hansen, R.J. Barthelmie, L.E. Jensen, A. Sommer, The impact of turbulence intensity and atmospheric stability on power deficits due to wind turbine wakes at Horns Rev wind farm, Wind Energy 15 (1) (2012) 183–196.
[8] R. Barthelmie, O.F. Hansen, K. Enevoldsen, J. Højstrup, S. Frandsen, S. Pryor, S. Larsen, M. Motta, P. Sanderhoff, Ten years of meteorological measurements for offshore wind farms, J. Sol. Energy Eng. 127 (2) (2005) 170–176.
[9] L. Vermeer, J.N. Sørensen, A. Crespo, Wind turbine wake aerodynamics, Prog. Aerosp. Sci. 39 (6) (2003) 467–510.
[10] I. Longley, M. Gallagher, J. Dorsey, M. Flynn, J. Barlow, Short-term measurements of airflow and turbulence in two street canyons in manchester, Atmos. Environ. 38 (1) (2004) 69–79.
[11] P. Chan, Atmospheric turbulence in complex terrain: verifying numerical model results with observations by remote-sensing instruments, Meteorol. Atmos. Phys. 103 (1–4) (2009) 145–157.
[12] D. Lenschow, J. Mann, L. Kristensen, How long is long enough when measuring fluxes and other turbulence statistics? J. Atmos. Ocean. Technol. 11 (3) (1994) 661–673.
[13] D.H. Lenschow, L. Kristensen, Uncorrelated noise in turbulence measurements, J. Atmos. Ocean. Technol. 2 (1) (1985) 68–81.
[14] P. Moriarty, J.S. Rodrigo, P. Gancarski, M. Chuchfield, J.W. Naughton, K.S. Hansen, E. Machefaux, E. Maguire, F. Castellani, L. Terzi, IEA-task 31 wakebench: towards a protocol for wind farm flow model evaluation. part 2: wind farm wake models, J. Phys. Conf. Ser. 524 (2014) 012185. IOP Publishing.
[15] A. Albers, H. Klug, D. Westermann, Power performance verification, in: EWEC-CONFERENCE 1-5 March, Nice, France, 1999, pp. 657–660.
[16] F. Zahle, N.N. Sørensen, Characterization of the unsteady flow in the nacelle region of a modern wind turbine, Wind Energy 14 (2) (2011) 271–283.
[17] S. Heier, Grid Integration of Wind Energy Conversion Systems, John Wiley & Sons, 1998, pp. 35–36. ISBN X 47197143.
[18] A. Sempreviva, R. Barthelmie, S. Pryor, Review of methodologies for offshore wind resource assessment in European seas, Surv. Geophys. 29 (6) (2008) 471–497.
[19] H. Jørgensen, S. Frandsen, P. Vølund, Analyses of Wake Effects on Middelgrunden Wind Farm, risø-r-1403, Risø National Laboratory, 2003. Tech. rep.
[20] S. Markkilde Petersen, Experimental Investigation of Gear Box Duration Loadings on Stall and Pitch Controlled Wind Turbines, Technical University of Denmark. Department of Fluid Mechanics, 1995, pp. 97–108.
[21] R.J. Barthelmie, S.T. Frandsen, M. Nielsen, S. Pryor, P.-E. Rethore, H. Jørgensen, Modelling and measurements of power losses and turbulence intensity in wind turbine wakes at Middelgrunden offshore wind farm, Wind Energy 10 (6) (2007) 517–528.
[22] M. J. Churchfield, S. Lee, J. Michalakes, P. J. Moriarty, A numerical study of the effects of atmospheric and wake turbulence on wind turbine dynamics, J. Turb. (13).
[23] T. Göçmen, P. van der Laan, P.-E. Réthoré, A.P. Diaz, G.C. Larsen, S. Ott, Wind Turbine Wake Models Developed at the Technical University of Denmark: a Review, Renew. Sustain. Energy Rev. 60 (2016) 752–769.
[24] S. Ott, Linearised CFD Models for Wakes, Denmark. Forskningscenter Risoe, 2011. Risoe-R, Danmarks Tekniske Universitet, Risø Nationallaboratoriet for Bæredygtig Energi.